Chemosphere 370 (2025) 143998

Contents lists available at ScienceDirect

Chemosphere

journal homepage: www.elsevier.com/locate/chemosphere

A biomarkers study of human skin fibroblasts exposition to glyphosate-based herbicide using an untargeted and targeted metabolomics approach

Josimar M. Batista [a], Dawidson A. Gomes [b], María J.G. Armijos [b], Michele A. Rodrigues [b], Helvécio C. Menezes [a], Zenilda L. Cardeal [a,*]

[a] Universidade Federal de Minas Gerais, Instituto de Ciências Exatas, Departamento de Química. Av. Antônio Carlos, 6627, Belo Horizonte, Minas Gerais, Brazil
[b] Universidade Federal de Minas Gerais, Instituto de Ciências Biológicas, Departamento de Bioquímica e Imunologia. Av. Antônio Carlos, 6627, Belo Horizonte, Minas Gerais, Brazil

HIGHLIGHTS

- Roundup glyphosate-based herbicide (GLYP-R) is cytotoxic to human dermal fibroblasts (HDFa) in a dose-dependent manner.
- GLYP-R induces oxidative stress in HDFa cells.
- GLYP-R can cause necrosis in HDFa cells.
- Methylcysteine and N-acetyl-L-methionine may indicate oxidative stress and aid cellular repair, suggesting GLYP-R exposure.

GRAPHICAL ABSTRACT

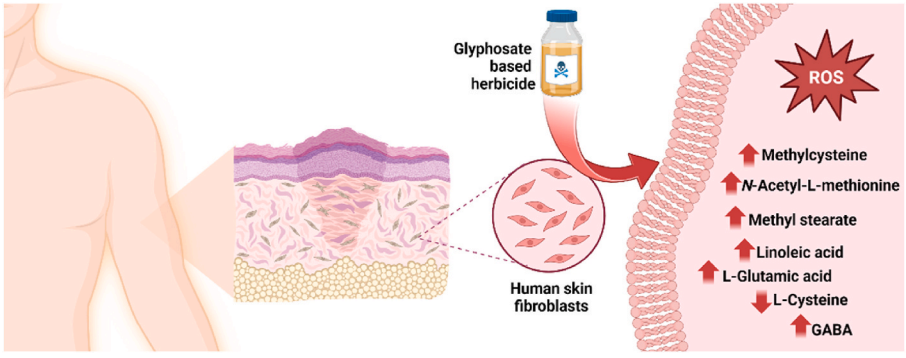

ARTICLE INFO

Handling Editor: A. Gies

Keywords:
Glyphosate-based herbicide
Metabolomics
Human fibroblasts
GC×GC
Chemometrics

ABSTRACT

Metabolomics is a valuable tool to assess glyphosate exposure and its potential impact on human health. However, few studies have used metabolomics to evaluate human exposure to glyphosate or glyphosate-based herbicides (GBHs). In this study, an untargeted and targeted metabolomics approach was applied to human skin fibroblasts exposed to the GBH Roundup (GLYP-R). Cytotoxicity, cell death, and oxidative stress assays were performed to evaluate potential damage caused by GLYP-R in fibroblasts. The herbicide showed a cytotoxic effect at concentrations above 100.0 mg L^{-1}, with IC_{50} = 164.2 ± 8.7 mg L^{-1}, inducing significant reactive oxygen species (ROS) production and necrosis. A GC×GC/Q-TOFMS method using derivatization with propyl chloroformate/propanol was developed for untargeted analysis, allowing the identification of 400 metabolites of different classes in the samples. The most significant compounds in the discrimination and classification of the samples were fatty acids and amino acids (AA). Based on the relevance of AA in untargeted analysis, a targeted analysis of 21 AA was performed using the same validated GC×GC method. Metabolomic analyses allowed the construction of two biomarker models with performance evaluated by receiver operating characteristic (ROC) curves: an untargeted model formed by four metabolites (methylcysteine, *N*-acetyl-L-methionine, methyl

* Corresponding author.
E-mail address: zenilda@ufmg.br (Z.L. Cardeal).

https://doi.org/10.1016/j.chemosphere.2024.143998
Received 29 October 2024; Received in revised form 16 December 2024; Accepted 18 December 2024
Available online 22 December 2024

stearate, and linoleic acid) and a targeted model formed by three AA (L-glutamic acid, L-cysteine, and γ-aminobutyric acid). This study is the first to report the use of metabolomics to evaluate human skin cells exposed to GLYP-R, contributing to the toxicological research on glyphosate.

1. Introduction

The herbicidal effect of glyphosate (GLYP) is based on its ability to disrupt the shikimate pathway, a metabolic pathway present exclusively in plants and bacteria. GLYP inhibits the enzyme 5-enolpyruvylshikimate-3-phosphate synthase (EPSPS) and suppresses the biosynthesis of amino acids, terpenoids, and other nutrients (Mesnage et al., 2021). As this pathway is absent in mammals, the herbicide was launched in the agriculture market as "not toxic to humans and animals". However, several recent studies have shown a relationship between exposure to GLYP and its commercial formulations (glyphosate-based herbicides, GBHs) with the development of neurotoxicity, reproductive toxicity, hepatotoxicity, nephrotoxicity, and carcinogenicity (X. Wang et al., 2022a,b). Roundup (GLYP-R) is the most well-known GBH. Studies have compared the toxicity of GLYP and GBHs such as GLYP-R and have shown that commercial formulations are generally more toxic to human and animal cells. The toxicity of GBHs is mainly due to the presence of surfactants such as polyoxyethylene amine (POEA), which facilitates cell membrane disruption (Mesnage et al., 2019; Song et al., 2012).

The possible mechanisms through which GLYP and GBHs affect human health are mainly associated with disturbances in the redox balance of cells and metabolic changes (X. Wang et al., 2022a,b). Richard et al. (2005) investigated the effects of exposure of human placenta cells (JEG-3) to Roundup and found that herbicide binds to the active sites of the aromatase enzyme, impairing estrogen synthesis. In addition, changes in mRNA levels have been identified. Damage to the epithelial membrane of the buccal epithelial cell line (TR146), impairment in mitochondrial functions, and genetic alterations have indicated that Roundup causes DNA damage (Koller et al., 2012). Mesnage et al. (2013) showed that GBHs cause changes in the mitochondrial activity of liver cells (Hep G2), inducing necrosis and endocrine disruption. In recent years, several other studies have investigated the toxicological modes of action of GLYP and GBHs through experiments involving human cells, animal cells, and the occupational exposure of workers (Gill et al., 2018; Nagy et al., 2019; Agostini et al., 2020; Martins-Gomes et al., 2022; Lacroix and Kurrasch, 2023). These studies have substantially contributed to a better understanding of the impacts of glyphosate on human health. Metabolomics can be used to evaluate the toxic effects of contaminants, which determine the set of metabolites (targeted or untargeted) of a living system subjected to exogenous or endogenous stimuli (Fiehn, 2002). Metabolites, such as AA, can act as biomarkers and can be used in biomolecular diagnosis, facilitating early detection and more efficient treatment of diseases. Several studies have investigated metabolomics and GLYP/GBHs, mainly in soil, animals, and plants (Petersen et al., 2011; Aristilde et al., 2017; Krause et al., 2020; Mesnage and Antoniou, 2022; B. Wang et al., 2022a,b; Hsiao et al., 2024). However, few studies have used metabolomics to evaluate the toxicity of GLYP and GBHs in humans (Magrì et al., 2021; Zhang et al., 2022). To the best of our knowledge, no metabolomic study has been conducted on the exposure of human skin cells to GLYP or GBHs. The skin is the largest organ in the human body and is exposed to the adverse effects of external agents such as pesticides.

Improved methods are essential for enhancing metabolite assessments. Comprehensive two-dimensional gas chromatography (GC×GC) has demonstrated excellent performance in metabolomics data acquisition, particularly in untargeted analysis (Miyazaki et al., 2017; Snow, 2020). Owing to the increased peak resolution, GC×GC allows the identification and quantification of a much larger number of compounds than one-dimensional gas chromatography (1D-GC). When used with sample preparation involving derivatization, GC×GC allows the analysis of low-volatile or non-volatile compounds, further increasing the number of metabolites determined. Derivatization using alkyl chloroformates (mainly methyl, ethyl, and propyl chloroformates) has become increasingly popular due to its effectiveness in an aqueous medium and its rapid processing. This method is more suitable for analyzing biological samples compared to traditional silylation, which requires an anhydrous environment and longer reaction times (Dettmer et al., 2012; Husek, 1998; Villas-Bôas et al., 2011).

Based on the importance of evaluating the toxicity of GLYP-R to human skin at the molecular level, the present study proposes a novel GC×GC method to identify biomarkers of herbicide exposure in human skin fibroblast cell cultures. The validated method was applied to both untargeted and targeted metabolomic (AA) analyses.

2. Materials and methods

2.1. Chemicals

Propyl chloroformate (PCF), 1-propanol, 3-methylpyridine, isooctane, phenol, thiodiethylene glycol, resazurin, hydrogen chloride, EDTA, sodium chloride, potassium chloride, Nonidet P-40, anhydrous calcium chloride and amino acid reference standards were obtained from Merck (Darmstadt, Germany). Phosphate buffer solution (PBS), Dulbecco's Modified Eagle Medium (DMEM), Hoechst 33342, propidium iodide (PI), Triton 100 × , fetal bovine serum (FBS), penicillin, streptomycin, amphotericin (PSA) and the Image-iT™ LIVE Green Reactive Oxygen Species Detection Kit (I36007) were obtained from Thermo Fisher Scientific (Massachusetts, USA). Chloroform, methanol, and acetonitrile were obtained from J. T. Baker (Hampton, USA). Sodium hydroxide was purchased from Panreac (Barcelona, Spain), ultrapure water from Elga (Lane End, UK), and ethyl alcohol from CRQ (SP, Brazil). Roundup Original DI was obtained from Monsanto/Bayer (Missouri, USA), Tris-base from Biosolve (Valkenswaard, Netherlands), and hexahydrate magnesium chloride from Dinâmica (SP, Brazil).

2.2. Biological assays

To evaluate the toxic effects of GLYP-R, a cytotoxicity assay using resazurin metabolization, cell death using PI labeling, and an oxidative stress assay in human skin fibroblasts were performed, as described in the Supplementary Material (SM). Human skin fibroblasts were selected for this study because of their relevance to human exposure to glyphosate-based herbicides (GLYP-R) via dermal contact. Fibroblasts are abundant in the dermis and play crucial roles in wound healing and tissue repair. Biological assays were performed at least in triplicate using different cell passages. Data were analyzed using GraphPad Prism 9, and the results are reported as graphs of the mean with standard deviation. One-way analysis of variance (ANOVA) was applied to the data to evaluate statistical differences ($p < 0.05$) between groups.

2.3. Quenching, cell harvesting, and metabolite extraction

The protocol for quenching, cell harvesting, and extraction of metabolites was adapted from Rodrigues et al. (2024). Some steps of the original protocol were modified after the univariate optimization tests, including cell lysis (comparing PBS and NETN buffers), extraction solvent (comparing methanol/acetonitrile, MeOH/ACN, 1:1 and methanol/chloroform/water, MeOH/$CHCl_3$/H2O, 7:2:1) and sample preconcentration (freeze-drying and no freeze-drying), as described in the SM.

2.4. GC × GC/Q-TOFMS system

Untargeted and targeted data were acquired using the GC × GC/Q-TOFMS system. An Agilent 7890B chromatograph coupled to a hybrid quadrupole time-of-flight mass spectrometer (Agilent 7250) manufactured in Wilmington (USA) was used. The modulator is a thermal loop-type modulator (Zoex, model ZX2) manufactured by Houston (USA). The system was equipped with Agilent MassHunter v. 10.2 (2023) software for the acquisition of raw chromatograms, GC Image v. 2.9r3 (2020) software for the acquisition and treatment of two-dimensional chromatograms and NIST 17 v. 2.3 (2017) library.

A single chromatographic method was optimized for both the untargeted and targeted analyses. The system used an HP-5MS 1D column (30 m × 250 μm × 0.25 μm) and the 2D Rxi-17Sil MS column (2 m × 0.15 mm × 0.15 μm). Injector temperature was 250 °C in splitless mode (0.5 min), with helium (1.2 mL min^{-1}) as carrier gas. The oven was heated from 80 °C (1 min) to 150 °C (2 min) at 5 °C min^{-1}, then to 270 °C (3 min) at 3 °C min^{-1}. The modulation period was 6 s, and the hot-jet duration was 1 s, with an offset of +30 °C relative to the oven. Nitrogen gas at −80 °C was used as the cold jet (20.0 L min^{-1}). The transfer line was operated at 240 °C, the ion source at 250 °C, and the quadrupole source at 150 °C. Ionization was performed using electron ionization (EI) at 70 eV in positive mode. The ions were acquired at 50 Hz in the full scan mode in the range of *m/z* 50–650. The detector was operated with a microchannel plate (MCP) at 800 V and a photomultiplier tube (PMT) at 551 V.

2.5. Metabolites derivatization

The metabolites were derivatized with propyl chloroformate/propanol, according to a previously described methodology (Batista et al., 2020).

2.6. Data processing

Two-dimensional chromatograms were processed using the GC Image software. Baseline correction was applied with parameters: deadband = 5, distribution = 7.00, median mean filter (size = 7), and strides per modulation cycle = 1. Spectral noise from spine bleeding was removed, and peaks with S/N > 100 were detected. Chromatograms were then aligned using a feature auto-template built via the consistent click method (CCD) algorithm (Reichenbach et al., 2013).

The aligned data were normalized to the features corresponding to L-norvaline (internal standard) and the protein mass of each extract. Protein measurements were performed according to the Bradford's protocol (Bradford, 1976). The data matrix was uploaded to MetaboAnalyst 6.0 website (Pang et al., 2024). The following tools from the Statistical Analysis [one factor] module were used: volcano plot (Univariate Analysis), Chemometrics Analysis (Principal Component Analysis, PCA and Partial Least Squares - Discriminant Analysis, PLS-DA), Cluster Analysis (dendrogram and heatmaps), and Classification and Feature Selection (Random Forest). These methods are used for the univariate and multivariate statistical analyses of metabolites, enabling the selection of biomarker candidates. In addition, the Biomarker Analysis module allowed the validation of the biomarker models through ROC analysis. Finally, Enrichment and Pathway Analysis modules were used to identify metabolic pathways associated with the altered metabolites.

2.7. Metabolites identification

The untargeted metabolites were identified by comparing the acquired mass spectra with the spectra from the NIST 17 library and the metabolomics database The Human Metabolome Database (HMDB) (Wishart et al., 2022). A match factor >750 was used. Additionally, the tentative identification of compounds relied on the retention index (*I*), calculated using the methodology developed by van Den Dool and Dec. Kratz (1963). The targeted metabolites (AA) were identified by comparing the spectra of the AA-derivatized analytical standards and the retention times with NIST 17 MS data.

2.8. Validation of the targeted GC×GC analysis

To validate the targeted GC×GC method, a mixture of 1.00 mg L^{-1} of 21 AA with reference materials was prepared in ultrapure water. This mixture was adequately diluted to construct the AA calibration range and validate the merit figures (SM). The figures evaluated were linearity, intermediate precision, repeatability, limit of detection (LOD), limit of quantification (LOQ), and recovery.

3. Results and discussion

To comprehensively investigate the effects of GLYP-R on fibroblasts, biological assays, untargeted/targeted metabolomics, and chemometrics were used together in this study. Fig. 1 illustrates the scheme of the approaches employed in this study.

3.1. GLYP-R induces cytotoxicity in HDFa cells in a dose-dependent manner

The commercial formulation Roundup is used in the agricultural sector at a final dilution of 1.0–2.0%, that corresponds to 3.7–7.4 g L^{-1} of glyphosate (original Roundup flask: 370 g L^{-1} of glyphosate) (de Melo et al., 2018). Thus, 400.0 mg L^{-1} of glyphosate (Roundup dilution of 0.11%) was chosen as the highest level of exposure to HDFa cells. Relative to the control group (−), GLYP-R concentrations below 100.0 mg L^{-1} were not toxic to the cells at any exposure time (Figs. S1–a). A 400.0 mg L^{-1} concentration exhibited the minimum % of resazurin metabolism (near zero at 24 and 48 h and zero at 72 h of exposure). This result suggests that this concentration significantly decreased cell viability, indicating that 400.0 mg L^{-1} exhibited the most pronounced cytotoxic effect in fibroblasts. There were no significant changes in the metabolic profile at 48 and 72 h (Fig. S1-c and d). Then, a 24 h exposure time was selected to estimate IC_{50} (Figs. S1–b) and was maintained in subsequent experiments. The positive control group proved to be efficient, not indicating cell viability, compared to the negative control group ($p < 0.0001$). The nonlinear regression model of the dose-dependence curve did not show a lack of fit ($p = 0.8566$), the distribution of residuals was homogeneous, and outliers were removed. The IC50 value was determined as 164.2 ± 8.7 mg L^{-1}, with a 95% confidence interval, and $R^2 = 0.9648$.

3.2. GLYP-R causes cell death by necrosis in HDFa

The resazurin assay indicated decreased viability of HDFa cells exposed to GLYP-R owing to a cytotoxic effect. However, a more specific assay using PI is needed to assess whether the cells have undergone cell death. The PI fluorescent probe penetrates cells with compromised cell membranes and does not penetrate the viable cells. This probe binds to DNA (which causes a 20–30 fold increase in fluorescence) and can indicate cell death by necrosis (Arndt-Jovin and Jovin, 1989). Hoechst dye marks all cell nuclei, whether viable or not. Cells exposed to GLYP-R and treated with PI were labeled, whereas cells that were not exposed to GLYP-R and treated with PI were not labeled (Figs. S2–a). GLYP-R induced necrosis in HDFa cells to 0% for control, 0.64 ± 0.07% for GLYP-R 50.0 mg L^{-1}, 13.00 ± 0.93% for IC_{50} and 100.2 ± 6.2% for GLYP-R 400 mg L^{-1} (Figs. S2–b). This result was confirmed by cell morphology analysis, which showed cell surface deformation at GLYP-R concentrations greater than 50.0 mg L^{-1}. Thus, 0.11% dilution of the commercial formulation was sufficient to cause complete death of human fibroblast cells. As demonstrated in the literature (Heu et al., 2012; Martini et al., 2012), the results of this study confirm that GLYP-R

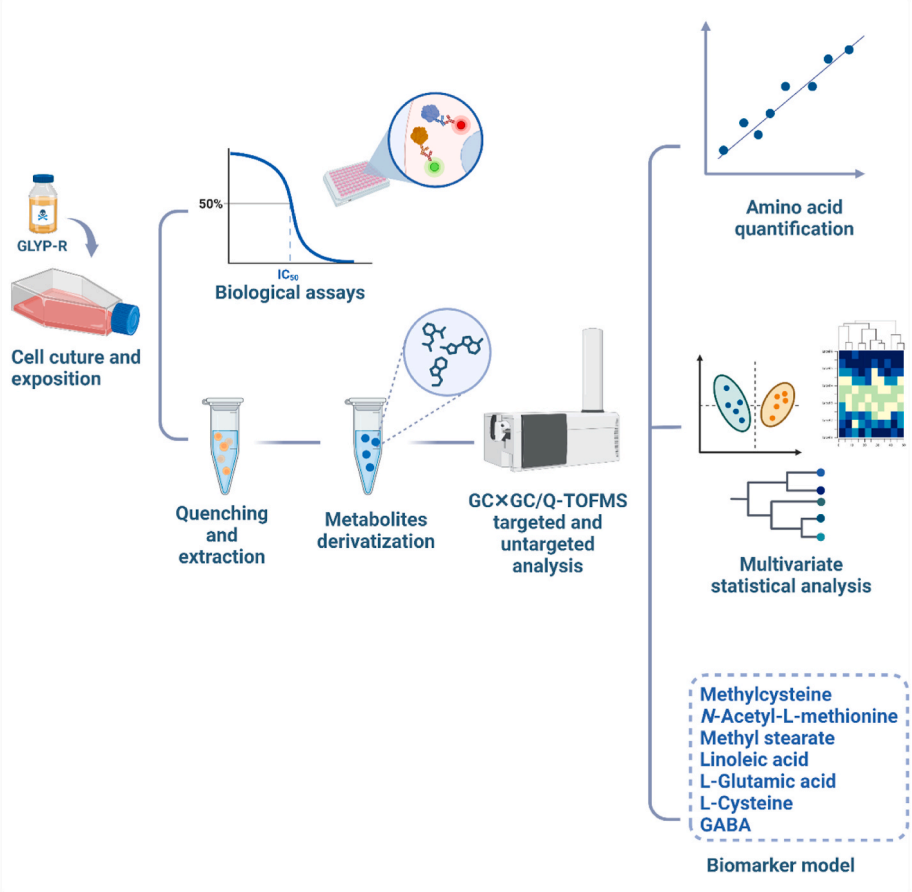

Fig. 1. Workflow of the tools used in the GLYP-R exposure study with human skin fibroblasts.

can be highly toxic to human skin, especially given that it is applied at concentrations approximately ten times higher than the maximum concentration assessed in this study.

3.3. *GLYP-R induces oxidative stress in HDFa cells*

In vitro studies in human cells (such as renal cells and hepatocytes) and in vivo studies in animals (such as Wistar rats and mice) have shown

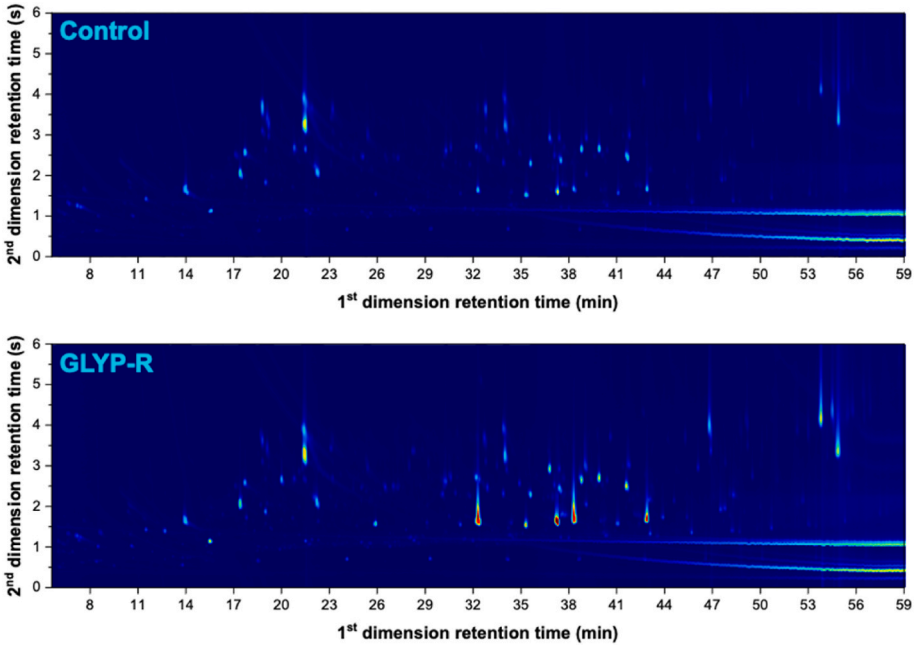

Fig. 2. Untargeted contour plots for derivatized extracts of cells not exposed (control) or exposed to GLYP-R.

that glyphosate is a causative agent of oxidative stress (X. Wang et al., 2022a,b). In the present study, human fibroblasts labeled with carboxy-H2DCFDA and exposed to GLYP-R emitted more significant fluorescence (approximately 800 times more) than labeled and unexposed cells (Fig. S3). The significant increase in fluorescence observed with GLYP-R treatment implied a large increase in ROS production. This result reinforces findings from existing literature on other biological models, while also revealing that GLYP-R induces oxidative stress in human skin fibroblasts.

3.4. GC×GC/Q-TOFMS untargeted analysis

The GC×GC method allowed the detection of 514 features in the analyzed samples. After artifact removal, like peaks associated with column bleeding, 400 metabolites were identified. Compound identification was performed using the retention index, NIST 17 library, and HMDB database (Table S2). There were no evident differences in the resolution of compounds between the control and treatment chromatograms. However, the peak intensity was higher for the cell extracts exposed to GLYP-R (Fig. 2).

3.5. Multivariate statistical analysis of untargeted metabolites

The results of comprehensive two-dimensional gas chromatographic analyses provide a large amount of data, which is desirable for untargeted metabolomics. However, comparisons were made to identify statistically significant patterns of metabolite variations relevant to the biological questions. In this context, chemometric tools are useful for reducing the dimensionality of the data acquired by GC×GC and for extracting useful information (Kubota et al., 2022). Thus, the peak intensity data of the 400 metabolites obtained by GC×GC analysis were pre-processed and analyzed using the open MetaboAnalyst 6.0.

After normalizing the peak intensities using L-norvaline (IS) and protein mass, the data matrix (25 samples × 400 features) was uploaded as ".csv" format with unpaired samples arranged in rows. The 25 samples were divided into two groups: the control group (metabolites from unexposed cells) and GLYP-R group (metabolites from cells exposed to GLYP-R. No missing values are detected. The interquartile range (IQR) filter, set to a threshold of 10%, was applied to exclude low-variance metabolites that contributed minimally to data variability. The preprocessing method that provided the best normal data distribution was Pareto scaling (Fig. S10). Using the Random Forest tool, sample C01 was identified as a potential outlier and removed from the dataset (Fig. S11). The data were then scaled again (Pareto scaling) to obtain a better Gaussian distribution (Fig. S12).

A heat map of the top 80 metabolites (Fig. S8) showed that the metabolites with the highest peak intensity values were associated with cell exposure to GLYP-R, suggesting increased biosynthesis of these metabolites compared to the control. Compounds of different chemical classes, particularly amino acids, fatty acids, alcohols, hydrocarbons, ketones, aldehydes, amines, and amides, were identified in the samples.

Initially, a univariate analysis was performed using a volcano plot to identify the most significant metabolites responsible for sample differentiation (Fig. S9). The analysis showed 227 metabolites that had a significant increase in peak intensity from the control to the GLYP-R group (negative side of the $\log_2$ FC-axis) and 18 metabolites that significantly decreased from the control to the GLYP-R group (positive side of the $\log_2$ FC-axis). Some metabolites that showed a large magnitude of change with a high statistical difference (higher values of $-\log p$ and log2 FC) are highlighted in the graph. Among them, some amino acids stood out, indicating that this group of biomolecules significantly influenced the statistical difference observed between the exposed and unexposed cell samples.

Subsequently, PCA was used to perform multivariate exploratory analysis of the data samples. A PCA model was constructed with normalized data, and it was observed that from the third PC onwards, there was no significant difference in the percentage of variance explained by the model (Fig. S13). The final model was built using three PCs, which provided 66.5% of the explained variance. The model showed the group scores along PC 1 (Fig. S14-a and b), allowing for a clear separation between the control and GLYP-R groups, indicating a statistical difference between cells exposed and not exposed to GLYP-R. The associated loadings enabled the identification of variables (metabolites) related to the observed clusters. The loadings of the positive part of PC 1 were associated with the exposed cell samples, whereas those of the negative axis of PC 1 were associated with the control samples (Figs. S14–c). The metabolites that discriminated the exposed cell samples were methylcysteine, *N*-acetyl-L-methionine, methyl stearate, and linoleic acid. The metabolite with the most negative loading, N-formyl-L-methionine, was responsible for the discrimination of control samples. The HCA model showed clustering of all control samples into one cluster and GLYP-R samples into the other (Figs. S14–d), indicating chemical similarity between the samples of each group and statistical differences in the relative amounts of metabolites between the groups.

Considering that information on which samples belonged to each group (control and GLYP-R) was known, the application of a supervised classification method (PLS-DA) to the dataset was possible. To choose the number of latent variables (LVs) of the model, leave-one-out (LOOCV) cross-validation was performed. The best model presented 2 LVs and was chosen based on the highest values of Q^2 (0.87838) and R^2 (0.93851). The values obtained for Q^2 and R^2 were close to 1, indicating that the model exhibited good predictive capacity and good fit (Figs. S15–a) (Szymańska et al., 2012). In addition, the model showed maximum accuracy (1.0), indicating 100% prediction (no sample was incorrectly classified). A permutation test was performed based on the separation distance (B/W) with 100 permutations to evaluate overfitting. As shown in Figs. S15–b, the calculated B/W distribution from the permutated data differed significantly from the B/W distribution based on the original data ($p < 0.01$). This result indicated that the model did not overfit. The model constructed with two LVs discriminated the samples into two groups along LV 1 (Figs. S15–c). The VIP scores of LV 1 indicated the variables that influenced sample discrimination (Figs. S15–d). The 5 top metabolites were methylcysteine, N-acetyl-L-methionine, methyl stearate, linoleic acid, and 3,4-methylenedioxybenzaldehyde (3,4-MDB). PLS-DA confirmed the PCA loading plot, suggesting that these metabolites were candidates for untargeted biomarkers of GLYP-R exposure.

3.6. Untargeted biomarkers model

Individuals who apply GLYP-R to crops or live near application areas are exposed to the herbicide through various routes, including skin contact, air and consumption of contaminated food or water (Helander et al., 2018; Li et al., 2016; Ramirez Haberkon et al., 2021). Therefore, identifying biomarkers of herbicide exposure can serve as an early and efficient diagnostic tool, helping in the prevention of late-stage diseases that are challenging to treat. Molecular diagnosis allows the discovery of the disease in its early stages, the application of less invasive forms of treatment and even increasing the patient's possibility of cure (Eve et al., 2021; Sreekumar et al., 2009). Using the biomarker analysis module of MetaboAnalyst, an untargeted biomarker model was evaluated for metabolites with the highest VIP scores on PLS-DA analysis.

Multivariate ROC curve-based exploratory analysis was performed to build sets of biomarkers (models) based on diagnostic performance (area under the ROC curve, AUC) and classification (sensitivity and specificity) parameters. Multivariate ROC curve analysis shows better performance values than classical univariate ROC curve analysis, which evaluates biomarkers individually (Chong et al., 2019; Zhang et al., 2022). ROC curves were generated using Monte Carlo cross-validation (MCCV) to avoid overfitting. In each MCCV, 2/3 of the samples (calibration set) were used to select the most significant features using

PLS-DA classification, with 2 LVs and 1/3 used to validate the model. This process was repeated several times to calculate the model performance parameters. Fig. 3-a shows the ROC curves based on the cross-validation performance for models with different amounts of metabolites. The MCCV chose the best model with ten features; however, the model with only four features also exhibited high diagnostic performance (AUC = 0.996). Using the AUC, the predicted classification probabilities of each sample were calculated (Fig. 3-b) using the 4-biomarker model. Based on the confounding matrix (from cross-validation), the sensitivity and selectivity were 0.923 and 1.000, respectively, indicating that the model performed well in classifying the samples. The four metabolites selected by ROC analysis to form the GLYP-R exposure biomarker model are shown in Fig. 3-c. Emphasis should be placed on methylcysteine and *N*-acetyl-L-methionine, which were selected in 100% of the cases by cross-validation, to confirm that these were the most critical metabolites in the discrimination of the samples. Applying ROC curves to analyze the data confirmed that the four metabolites identified by the PLS-DA model were potential biomarkers. Since the current study took place in vitro with a specific skin cell line, the four metabolites could be candidate biomarkers of GLYP-R exposure. For use as biomarkers in clinical trials, additional validation steps involving other cell lines, animal models, and human models are necessary.

3.7. Biological interpretation of untargeted analysis

Enrichment and pathway analyses were performed using MetaboAnalyst to identify the most critical metabolic pathways linked to the metabolites identified in HDFa cells. The SMPDB library was used for the enrichment analysis (99 metabolite sets based on normal human metabolic pathways). This type of analysis is based on a global test tool that tests associations between sets of metabolites to establish their representative metabolic pathways (Goeman et al., 2004). The 25 metabolites with the highest VIP scores from the PLS-DA model, including the 10 untargeted biomarkers, were uploaded, and the results are shown in Fig. S16.

Several pathways have been identified, as illustrated in the network exhibited in Figs. S16–a and are detailed in Table S3. Nodes in the network represent metabolic pathways that share over 20% of their metabolites, such as glutamate metabolism, which shows strong interactions with aspartate metabolism, arginine and proline metabolism, nicotinate and nicotinamide metabolism, and the citric acid cycle. The size of each circle corresponds to the fold enrichment and the color indicates the p-value. Arginine and proline metabolism showed the most significant fold enrichment (lower p-value), followed by the metabolism of ketone bodies, alpha-linolenic acid, linoleic acid, and biosynthesis of spermidine and spermine (Fig. S16-b and c). These two metabolic pathways were the most important in the differentiation of cell samples exposed and not exposed to GLYP-R, and consequently, in the explanation of the biomarker model.

Pathway Analysis using the KEGG library (for Homo sapiens) confirmed the enrichment analysis, with arginine and proline metabolism being the most important biological explanation for the set of significant metabolites (Fig. S17, Table S5). Phenylalanine, tyrosine, and tryptophan biosynthesis, as well as linoleic acid metabolism, also contribute to the biological effects of GLYP-R exposure on HDFa cells.

Methylcysteine is an amino acid biosynthesized by cysteine methylation and is known to act as a protective agent against oxidative stress, which causes DNA damage (Rubino et al., 2011). Cysteine metabolism is associated with arginine and proline pathways through the spermine intermediate, which was identified in this study. Cysteine and methionine metabolism produces *S*-adenosylmethioninamine from *S*-adenosyl-L-methionine via *S*-adenosylmethionine decarboxylase. *S*-adenosylmethioninamine is then converted to spermine via the

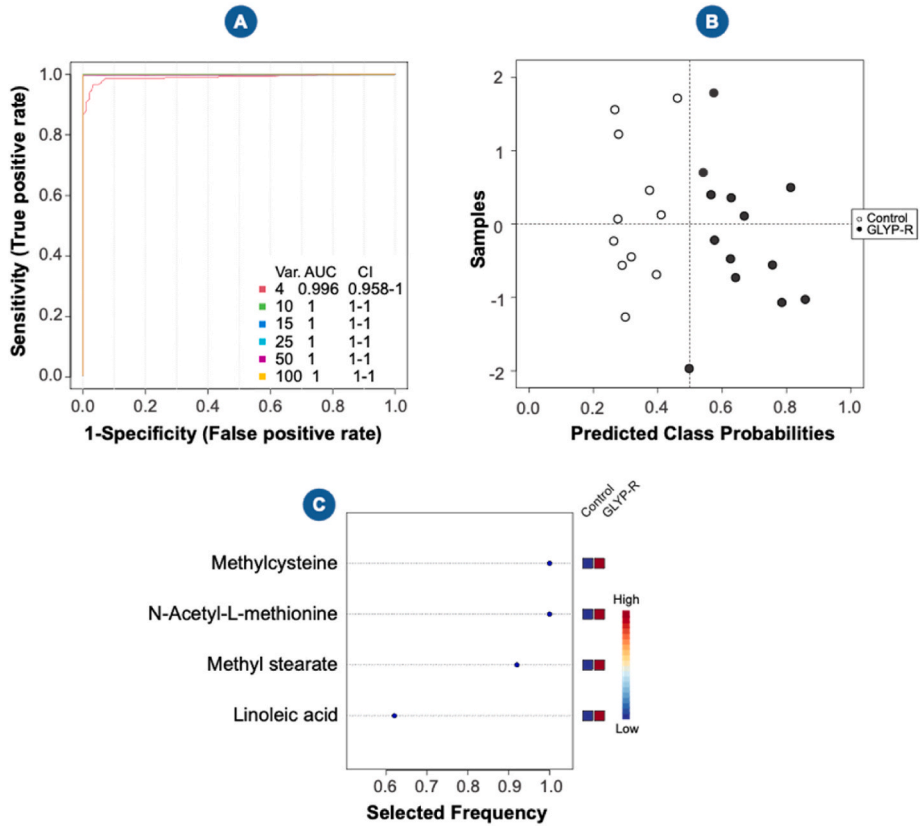

Fig. 3. Untargeted biomarker model in HDFa cells exposed to GLYP-R. ROC curves for models with different numbers of biomarkers (a). The classification prediction plot shows that only one sample was incorrectly classified (b). Four metabolites of biomarker model (c). n(GLYP-R) = 13, n(control) = 11.

enzyme spermine synthase (KEGG, 2024a). In the present study, methylcysteine was up-regulated in cells exposed to GLYP-R (Fig. S18). This indicated that the herbicide caused oxidative stress in HDFa cells, as confirmed by the oxidative stress assay (topic 3.3). The formation of methylcysteine has already been related to the repair of O^6-methylguanine DNA lesions caused by *N*-nitroso compounds in human fibroblast cells (Harris et al., 1984). This type of DNA injury is related to mutagenic and carcinogenic effects. Thus, the high regulation of methylcysteine also suggests the induction of carcinogenesis by glyphosate, as already indicated in the literature (Hao et al., 2019; Mink et al., 2012; Roma et al., 2023).

The second most significant metabolite, *N*-acetyl-L-methionine, is also an AA derivative known to inhibit ROS production (Kouno et al., 2014) and is upregulated in cells exposed to GLYP-R. This metabolite can be biosynthesized by the degradation of *N*-acetylated proteins via specific hydrolases or by direct synthesis from AA methionine through specific *N*-acetyltransferases (KEGG, 2024b). Like cysteine, methionine metabolism is connected to arginine and proline pathways by the spermine intermediate. Wang et al. (2023) identified *N*-acetyl-L-methionine as a potential biomarker for the diagnosis of Alzheimer's disease and mild cognitive impairment. Some studies have linked exposure to glyphosate to the development of neurodegenerative diseases (Ignácio et al., 2024; Ren et al., 2024; Winstone et al., 2022). The upregulation of *N*-acetyl-L-methionine observed in the present study suggests that this metabolite may be used as a biomarker for the development of neurodegenerative diseases related to glyphosate exposure.

Methyl stearate is a fatty acid methyl ester obtained from stearic acid, which, in turn, is produced by the fatty acid biosynthesis pathway related to lipid metabolism. This pathway is responsible for cellular bioenergetics and plasma membrane integrity. Originating from acetyl-CoA, the biosynthesis of stearic acid occurs through a series of steps that end in the conversion of stearoyl-[acyl-carrier protein (ACP)] to stearic acid by the action of fatty acyl-ACP thioesterase A (KEGG, 2024c). The relationship between stearic acid (or its derivatives) and GLYP-R exposure remains unexplored. However, it is interesting to highlight that this fatty acid has already been associated with the development of coronary microvascular disease in a study involving postmenopausal women (Eve et al., 2021). This metabolite has also been identified as a potential autophagy inhibitor, a dysfunction closely related to Parkinson's disease. In addition, associations between the upregulation of stearic acid, chronic kidney disease (Zhang et al., 2016) and morbid obesity (Sansone et al., 2016) have already been reported.

Linoleic acid plays a central role in lipid metabolism, as it forms essential fatty acids, such as arachidonic acid, and is present in several other regulatory pathways (arachidonic acid metabolism, biosynthesis of unsaturated fatty acids, ferroptosis, necroptosis, regulation of lipolysis in adipocytes, and aldosterone synthesis and secretion) (KEGG, 2024d). Linoleic acid is metabolized to arachidonic acid by the γ-linolenate and dihomo-γ-linolenate intermediates. The higher amount of linoleic acid in the exposed cells compared to that in the control cells indicates the upregulation of arachidonic acid by exposure to GLYP-R. Arachidonic acid produces excess ROS in the cells and induces oxidative stress (Cheng et al., 2022). This compound activates calcium channels in the cell membrane via NOX2 (NADPH oxidase 2). The increasing Ca^{2+} concentration in the cytoplasm activates CPLA2 (cytosolic phospholipase A2), which, in the presence of arachidic acid, activates LOX (arachidonate 15-lipoxygenase), generating high ROS production. Excess ROS increases membrane permeability in a process known as necroptosis (programmed necrosis) (KEGG, 2024e). The PI labeling assay indicated that GLYP-R induced cell death via necrosis in fibroblasts. However, PI labeling alone does not differentiate between the types of necrosis (programmed or unprogrammed) that occur in cells under stress. Future studies could clarify this by employing pharmacological inhibitors to selectively block or delay apoptosis, necroptosis, or ferroptosis while not affecting unscheduled necrosis (Costigan et al., 2023). Despite this, the upregulation of linoleic acid, with a consequent increase in the biosynthesis of arachidic acid, suggests that the necroptosis mechanism is involved in the cell death effect induced by herbicide exposure.

3.8. Targeted biomarkers model

The multivariate ROC curve method was applied to quantified AA with higher VIP scores of the PLS-DA model described in SM to evaluate the performance of AAs as targeted biomarkers (Fig. 4). The analysis showed that the model with the three biomarkers demonstrated high diagnostic performance (AUC = 0.921), with high sensitivity (1.000) and specificity (0.833). Using these adequate diagnostic and classification performance values, a targeted biomarker model was established comprising Glu, Cys, and GABA, with Glu highlighted as the most important biomarker in the model.

3.9. Biological interpretation of targeted analysis

Pathway analysis showed that amino acids exerted a solid contribution to the metabolic interpretation, considering that the most critical pathway in this study was arginine and proline metabolism, which are interconnected with several other pathways involving AA (alanine, aspartate, and glutamate metabolism; D-amino acid metabolism; lysine degradation; cysteine and methionine metabolism; glycine, serine, and threonine metabolism; glycine metabolism; and citrate cycle) (KEGG, 2024a). The AA L-glutamic acid (Glu) deserves direct discussion mainly because it regulates excessive ROS production (oxidative stress). The principal protective intracellular agent against oxidative stress is the tripeptide glutathione (GSH). In a reversible process, GSH reacts with free radicals and H_2O_2, oxidizing it to GSSG. Upregulation of GSH biosynthesis and decreased GSH/GSSG ratio indicate oxidative stress (Hayes and McLellan, 1999; Marrocco et al., 2017). The biosynthesis of GSH has as precursors Glu and L-cysteine (Cys), which are initially converted into L-γ-glutamylcysteine by the action of the glutamate-cysteine ligase catalytic subunit (GCLC). This intermediate then generates GSH through glutathione synthase (GSS). Although Glu is consumed in the biosynthesis of GSH, it is also produced during the catabolism of GSH to mercapturic acid (KEGG, 2024f). This evidence justifies the upregulation of Glu in cells exposed to GLYP-R in the present study (Fig. S24), confirming its role in protecting cells against the effects of oxidative stress (Zhang et al., 2022). The consumption of Cys in this process and the biosynthesis of methylcysteine (topic 3.7) justify its decrease in exposed cell samples compared to the control.

GABA was the third most crucial AA in the targeted biomarker model. This AA participates in several critical cellular metabolic pathways. GABA can be biosynthesized from Glu through glutamate decarboxylase (GAD) during alanine, aspartate, and glutamate metabolism (KEGG, 2024g). GABA produces succinate as its final metabolite through a two-step process that enters the citrate cycle. This AA can also be produced from L-arginine (Arg) or L-proline (Pro), which have ornithine as a common intermediate in the arginine and proline metabolism pathways. GABA metabolism also produces acetyl-CoA (responsible for initiating the citrate cycle) in several reversible steps. Thus, this AA is essential for maintaining cellular energy mechanisms. GABA is traditionally known as an inhibitory neurotransmitter in the central nervous system (Roberts, 1974). While its role in non-neuronal tissues is not well understood, studies have confirmed the synthesis of GABA in the pancreas, stomach, and testicles (Gilon et al., 1991; Tillakaratne et al., 1992). In a study by Ito et al. (2007), the localization and characterization of GAD in human and rat skin fibroblast revealed that GABA stimulated hyaluronic acid synthesis and increased protection against oxidative stress in cells. This finding supports our observation of GABA upregulation in human fibroblasts exposed to GLYP-R.

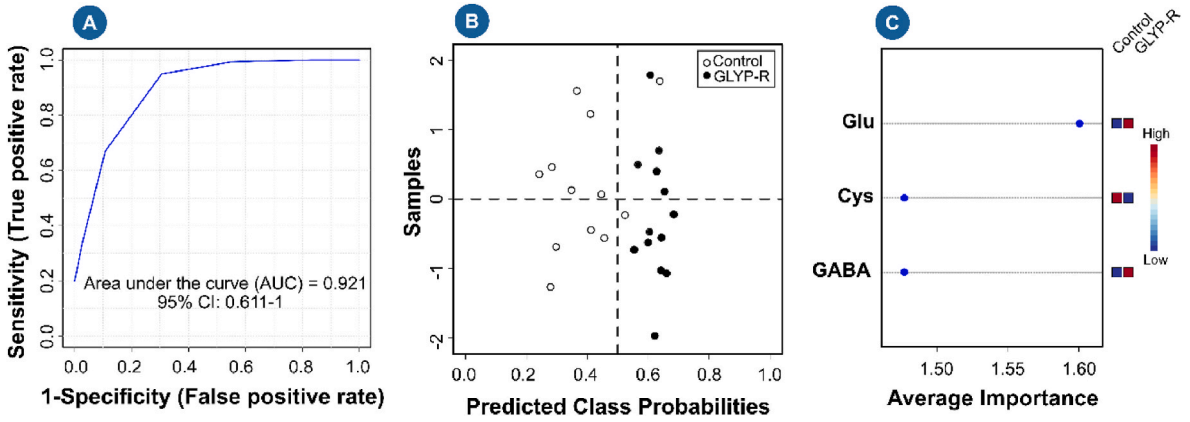

Fig. 4. ROC plot results: (a) diagnostic performance evaluation with AUC, (b) sample classification performance, and (c) importance of each AA in the targeted biomarker model of GLYP-R exposure; *n*(GLYP-R) = 13 and *n*(control) = 12.

3.10. Final remarks

The biomarkers identified in this study, particularly methylcysteine and *N*-acetyl-L-methionine, are associated with oxidative stress and cellular repair mechanisms. Although these biomarkers may be upregulated in response to various toxicants that induce oxidative stress, their specific pattern of change in combination with other metabolic alterations could potentially serve as a unique fingerprint for GLYP-R exposure.

However, the general principle of using metabolic changes as biomarkers of toxicity is well-established. Regardless of their specific mode of action, many toxicants can induce oxidative stress, disrupt metabolic pathways, or alter cellular homeostasis. Therefore, it is plausible that these or similar biomarkers could be useful for assessing exposure to a wider range of toxicants.

Glyphosate-based herbicides (GBHs), primarily targeting the shikimate pathway in plants, can also impact human metabolism. Although humans lack this pathway, GBHs can interfere with various metabolic processes. They induce oxidative stress by disrupting mitochondrial function and increasing ROS generation, which leads to cellular damage and inflammation (Abdelmagid et al., 2023; Martínez et al., 2020). Additionally, GBHs can affect amino acid metabolism, potentially affecting neurotransmitter synthesis and neurotransmission (Limberger et al., 2020). Furthermore, they can interfere with fatty acid metabolism, alter lipid profiles, and affect cellular membrane functions and energy production (Ford et al., 2017; Peillex and Pelletier, 2020). Metabolic disruptions caused by GBHs have broader health implications (Peillex and Pelletier, 2020). Long-term health effects of low-dose exposure, detailed mechanistic studies, and population studies are crucial to assessing the risks and developing effective strategies to minimize exposure. By understanding the complex mechanisms of GBH toxicity, we can protect public health and implement measures to reduce the use of potentially harmful herbicides.

The in vitro nature of this study limits its ability to fully capture the complex in vivo biological responses and systemic effects of glyphosate exposure on the skin. Additionally, the specific concentrations and exposure durations used may not fully reflect real-world skin exposure scenarios. Further research is needed to elucidate the precise mechanisms underlying the toxic effects of glyphosate-based herbicides on skin cells, including their role in oxidative stress, inflammation, and DNA damage. In vivo studies, such as animal models with dermal exposure, can provide valuable insights into the systemic effects of glyphosate exposure on the skin and inform risk assessments. Epidemiological studies can be used to assess the long-term health impacts of glyphosate exposure on human skin. Developing more accurate methods for assessing human skin exposure to glyphosate-based herbicides, such as biomonitoring studies, is crucial for risk assessment and regulatory decision making.

4. Conclusion

In this study, a single targeted and untargeted GC×GC/Q-TOFMS method was developed to analyze the metabolites in cell extracts. The method proved to be comprehensive in analyzing several classes of metabolites and had suitable validation parameters for AA analysis. Using in vitro biological assays, we showed for the first time that GLYP-R induces oxidative stress in human skin fibroblasts, causing cell death by necrosis. In addition, through targeted and untargeted metabolomics, we proposed potential biomarkers of human exposure to GLYP-R, comprising seven metabolites: methylcysteine, *N*-acetyl-L-methionine, methyl stearate, linoleic acid, L-glutamic acid, L-cysteine, and γ-aminobutyric acid. Through the analysis of metabolic pathways, combined with biochemical discussion, the modes of action of the biomarkers were interpreted, demonstrating their relationship with several essential pathways for energy metabolism and maintenance of cell life. This study makes significant contributions to the field of glyphosate toxicology, highlighting the increased risks of human exposure to GLYP-R, particularly through dermal contact.

CRediT authorship contribution statement

Josimar M. Batista: Writing – original draft, Validation, Methodology, Investigation, Formal analysis, Data curation. **Dawidson A. Gomes:** Writing – review & editing, Investigation, Data curation, Conceptualization. **María J.G. Armijos:** Writing – original draft, Formal analysis, Data curation. **Michele A. Rodrigues:** Writing – original draft, Formal analysis, Data curation. **Helvécio C. Menezes:** Writing – review & editing, Validation, Data curation, Conceptualization. **Zenilda L. Cardeal:** Writing – review & editing, Supervision, Project administration, Methodology, Funding acquisition, Conceptualization.

Declaration of competing interest

The authors declare the following financial interests/personal relationships which may be considered as potential competing interests: Zenilda L Cardeal reports financial support was provided by National Council for Scientific and Technological Development. Josimar M Batista reports financial support was provided by Coordination of Higher Education Personnel Improvement. Helvecio C Menezes reports financial support was provided by Minas Gerais State Foundation of Support to the Research. If there are other authors, they declare that they have no known competing financial interests or personal relationships that could have appeared to influence the work reported in this paper.

Acknowledgments

The authors would like to thank Fundação de Amparo à Pesquisa do Estado de Minas Gerais (FAPEMIG: APQ-01618-18; APQ-02135-24), Coordenação de Aperfeiçoamento de Pessoal de Nıvel Superior (CAPES), Conselho Nacional de Desenvolvimento Científico e Tecnológico (CNPq: 313729/2021-2, 442098/2023-5, 307998/2022–3), Rede Mineira de Engenharia de Tecidos e Terapia Celular (REMETTEC; RED00213-23; FAPEMIG), Rede Mineira de Pesquisa Translational em Oncologia (RED00059-23; FAPEMIG), and National Institutes of Health (NIH; grant 1R03TW008709) to support this work.

Appendix A. Supplementary data

Supplementary data to this article can be found online at https://doi.org/10.1016/j.chemosphere.2024.143998.

Data availability

Data will be made available on request.

References

Abdelmagid, A.D., Said, A.M., Abd El-Gawad, E.A., Shalaby, S.A., Dawood, M.A.O., 2023. Glyphosate-induced liver and kidney dysfunction, oxidative stress, immunosuppression in Nile tilapia, but ginger showed a protection role. Vet. Res. Commun. 47, 445–455. https://doi.org/10.1007/s11259-022-09961-0.

Agostini, L.P., Dettogni, R.S., dos Reis, R.S., Stur, E., dos Santos, E.V.W., Ventorim, D.P., Garcia, F.M., Cardoso, R.C., Graceli, J.B., Louro, I.D., 2020. Effects of glyphosate exposure on human health: insights from epidemiological and in vitro studies. Sci. Total Environ. 705. https://doi.org/10.1016/j.scitotenv.2019.135808.

Aristilde, L., Reed, M.L., Wilkes, R.A., Youngster, T., Kukurugya, M.A., Katz, V., Sasaki, C.R.S., 2017. Glyphosate-induced specific and widespread perturbations in the metabolome of soil Pseudomonas species. Front. Environ. Sci. 5, 266266. https://doi.org/10.3389/FENVS.2017.00034/BIBTEX.

Arndt-Jovin, D.J., Jovin, T.M., 1989. Fluorescence labeling and microscopy of DNA. In: Taylor, D.L., Wang, Y.L.B.T.M., C, B. (Eds.), Fluorescence Microscopy of Living Cells in Culture Part B. Quantitative Fluorescence Microscopy—Imaging and Spectroscopy. Academic Press, pp. 417–448. https://doi.org/10.1016/S0091-679X(08)60989-9.

Batista, J.M., Neves, M.J., Pereira, A.G., Gonçalves, L.S., Menezes, H.C., Cardeal, Z.L., 2020. Metabolomic studies of amino acid analysis in Saccharomyces cells exposed to selenium and gamma irradiation. Anal. Biochem. 597, 113666. https://doi.org/10.1016/j.ab.2020.113666.

Bradford, M.M., 1976. A rapid and sensitive method for the quantitation of microgram quantities of protein utilizing the principle of protein-dye binding. Anal. Biochem. 72, 248–254. https://doi.org/10.1016/0003-2697(76)90527-3.

Cheng, X., Chu, J., Zhang, L., Suo, Z., Tang, W., 2022. Intracellular and extracellular untargeted metabolomics reveal the effect of acute uranium exposure in HK-2 cells. Toxicology 473, 153196. https://doi.org/10.1016/j.tox.2022.153196.

Chong, J., Wishart, D.S., Xia, J., 2019. Using MetaboAnalyst 4.0 for comprehensive and integrative metabolomics data analysis. Curr. Protoc. Bioinforma. 68, 1–128. https://doi.org/10.1002/cpbi.86.

Costigan, A., Hollville, E., Martin, S.J., 2023. Discriminating between apoptosis, necrosis, necroptosis, and ferroptosis by microscopy and flow cytometry. Curr. Protoc. 3, e951. https://doi.org/10.1002/cpz1.951.

de Melo, M.I.A., Cunha, P. da S., Martins, T.M. da M., de Miranda, M.C., Gomes, D.A., de Goes, A.M., Novato-Silva, E., 2018. Glyphosate-based herbicide induces toxic effects on human adipose-derived mesenchymal stem cells grown in human plasma. Comp. Clin. Path. 27, 989–1000. https://doi.org/10.1007/s00580-018-2692-7.

Dettmer, K., Stevens, A.P., Fagerer, S.R., Kaspar, H., Oefner, P.J., 2012. Amino acid analysis. Methods in Molecular Biology. Humana Press, Totowa, NJ. https://doi.org/10.1007/978-1-61779-445-2.

Eve, A.A., Tunc, E., Liu, Y.J., Agrawal, S., Yilmaz, H.E., Emren, S.V., Akçay, F.A., Mainzer, L., Žurauskienė, J., Erdogan, Z.M., 2021. Identification of circulating diagnostic biomarkers for coronary microvascular disease in postmenopausal women using machine-learning techniques. Metabolites 11, 339. https://doi.org/10.3390/METABO11060339/S1.

Fiehn, O., 2002. Metabolomics–the link between genotypes and phenotypes. Plant Mol. Biol. 48, 155–171.

Ford, B., Bateman, L.A., Gutierrez-Palominos, L., Park, R., Nomura, D.K., 2017. Mapping proteome-wide targets of glyphosate in mice. Cell Chem. Biol. 24, 133–140. https://doi.org/10.1016/j.chembiol.2016.12.013.

Gill, J.P.K., Sethi, N., Mohan, A., Datta, S., Girdhar, M., 2018. Glyphosate toxicity for animals. Environ. Chem. Lett. 16, 401–426. https://doi.org/10.1007/s10311-017-0689-0.

Gilon, P., Tappaz, M., Remacle, C., 1991. Localization of GAD-like immunoreactivity in the pancreas and stomach of the rat and mouse. Histochemistry 96, 355–365. https://doi.org/10.1007/BF00271357.

Goeman, J.J., van de Geer, S.A., de Kort, F., van Houwelingen, H.C., 2004. A global test for groups of genes: testing association with a clinical outcome. Bioinformatics 20, 93–99. https://doi.org/10.1093/bioinformatics/btg382.

Hao, Y., Chen, H., Xu, W., Gao, J., Yang, Y., Zhang, Y., Tao, L., 2019. Roundup® confers cytotoxicity through DNA damage and Mitochondria-Associated apoptosis induction. Environ. Pollut. 252, 917–923. https://doi.org/10.1016/J.ENVPOL.2019.05.128.

Harris, C.C., Pegg, A.E., Grafstrom, R.C., Trump, B.F., 1984. O6-alkylguanine-DNA alkyltransferase activity in normal human tissues and cells. Cancer Res. 44, 2855–2857.

Hayes, J.D., McLellan, L.I., 1999. Glutathione and glutathione-dependent enzymes represent a co-ordinately regulated defence against oxidative stress. Free Radic. Res. 31, 273–300. https://doi.org/10.1080/10715769900300851.

Helander, M., Saloniemi, I., Omacini, M., Druille, M., Salminen, J., Saikkonen, K., 2018. Glyphosate decreases mycorrhizal colonization and affects plant-soil feedback. Sci. Total Environ. 642, 285–291. https://doi.org/10.1016/j.scitotenv.2018.05.377.

Heu, C., Elie-Caille, C., Mougey, V., Launay, S., Nicod, L., 2012. A step further toward glyphosate-induced epidermal cell death: involvement of mitochondrial and oxidative mechanisms. Environ. Toxicol. Pharmacol. 34, 144–153. https://doi.org/10.1016/j.etap.2012.02.010.

Hsiao, Y.C., Johnson, G., Yang, Y., Liu, C.W., Feng, J., Zhao, H., Moy, S.S., Harper, K.M., Lu, K., 2024. Evaluation of neurological behavior alterations and metabolic changes in mice under chronic glyphosate exposure. Arch. Toxicol. 98, 277–288. https://doi.org/10.1007/s00204-023-03622-0.

Husek, P., 1998. Chloroformates in gas chromatography as general purpose derivatizing agents. J. Chromatogr. B Biomed. Appl. 717, 57–91. https://doi.org/10.1016/S0378-4347(98)00136-4.

Ignácio, A. da C., Guerra, A.M., dos, R., de Souza-Silva, T.G., Carmo, M.A.V. do, Paula, H. A. de A., 2024. Effects of glyphosate exposure on intestinal microbiota, metabolism and microstructure: a systematic review. Food Funct. 15, 7757–7781. https://doi.org/10.1039/D4FO00660G.

Ito, K., Tanaka, K., Nishibe, Y., Hasegawa, J., Ueno, H., 2007. GABA-synthesizing enzyme, GAD67, from dermal fibroblasts: evidence for a new skin function. Biochim. Biophys. Acta - Gen. Subj. 1770, 291–296. https://doi.org/10.1016/j.bbagen.2006.09.017.

Kyoto Encyclopedia of Genes and Genomes (KEGG), 2024a. Arginine and proline metabolism - reference pathway. https://www.kegg.jp/pathway/map00330. accessed 28 August 2024.

The Human Metabolome Database (HMBD), 2024b. N-Acetyl-L-methionine. URL. https://hmdb.ca/metabolites/HMDB0011745, 8.28.24.

Kyoto Encyclopedia of Genes and Genomes (KEGG), 2024c. Arachidonic acid. URL https://www.kegg.jp/entry/C00219 (accessed 28 August 2024).

KEGG, 2024d. Arachidonic acid [WWW document]. Kyoto encycl. Genes Genomes. URL. https://www.kegg.jp/pathway/map04217+C00219, 8.28.24.

Kyoto Encyclopedia of Genes and Genomes (KEGG), 2024e. Glutathione metabolism - reference pathway. https://www.kegg.jp/pathway/map00480+C00051 (accessed 29 August 2024).

Kyoto Encyclopedia of Genes and Genomes (KEGG), 2024f. Alanine, aspartate and glutamate metabolism - reference pathway. https://www.kegg.jp/pathway/map00250+C00334 (accessed 9 October 2024).

Koller, V.J., Fürhacker, M., Nersesyan, A., Mišík, M., Eisenbauer, M., Knasmueller, S., 2012. Cytotoxic and DNA-damaging properties of glyphosate and Roundup in human-derived buccal epithelial cells. Arch. Toxicol. 86, 805–813. https://doi.org/10.1007/s00204-012-0804-8.

Kouno, Y., Anraku, M., Yamasaki, K., Okayama, Y., Iohara, D., Ishima, Y., Maruyama, T., Kragh-Hansen, U., Hirayama, F., Otagiri, M., 2014. N-acetyl-l-methionine is a superior protectant of human serum albumin against photo-oxidation and reactive oxygen species compared to N-acetyl-l-tryptophan. Biochim. Biophys. Acta - Gen. Subj. 1840, 2806–2812. https://doi.org/10.1016/j.bbagen.2014.04.014.

Krause, J.L., Haange, S.B., Schäpe, S.S., Engelmann, B., Rolle-Kampczyk, U., Fritz-Wallace, K., Wang, Z., Jehmlich, N., Türkowsky, D., Schubert, K., Pöppe, J., Bote, K., Rösler, U., Herberth, G., von Bergen, M., 2020. The glyphosate formulation Roundup® LB plus influences the global metabolome of pig gut microbiota in vitro. Sci. Total Environ. 745, 140932. https://doi.org/10.1016/J.SCITOTENV.2020.140932.

Kubota, L.T., da Silva, J.A.F., Sena, M.M., Alves, W.A. (Eds.), 2022. Tools and Trends in Bioanalytical Chemistry. Springer International Publishing, Cham. https://doi.org/10.1007/978-3-030-82381-8.

Lacroix, R., Kurrasch, D.M., 2023. Glyphosate toxicity: in vivo, in vitro, and epidemiological evidence. Toxicol. Sci. 192, 131–140. https://doi.org/10.1093/toxsci/kfad018.

Li, M.H., Xu, H.D., Liu, Y., Chen, T., Jiang, L., Fu, Y.H., Wang, J.S., 2016. Multi-tissue metabolic responses of goldfish (: Carassius auratus) exposed to glyphosate-based herbicide. Toxicol. Res. 5, 1039–1052. https://doi.org/10.1039/c6tx00011h.

Limberger, C., Ferreira, P.C.L., Fontella, F.U., Oliveira, A.C.L.J., Salles, G.B., Souza, D.O., Zimmer, E.R., de Souza, D.G., 2020. Glyphosate-based herbicide alters brain amino acid metabolism without affecting blood-brain barrier integrity. Alzheimer's Dement. 16. https://doi.org/10.1002/alz.043847.

Magrì, D., Veronesi, M., Sánchez-Moreno, P., Tolardo, V., Bandiera, T., Pompa, P.P., Athanassiou, A., Fragouli, D., 2021. PET nanoplastics interactions with water contaminants and their impact on human cells. Environ. Pollut. 271. https://doi.org/10.1016/j.envpol.2020.116262.

Marrocco, I., Altieri, F., Peluso, I., 2017. Measurement and clinical significance of biomarkers of oxidative stress in humans. Oxid. Med. Cell. Longev. 2017. https://doi.org/10.1155/2017/6501046.

Martínez, M.-A., Rodríguez, J.-L., Lopez-Torres, B., Martínez, M., Martínez-Larrañaga, M.-R., Maximiliano, J.-E., Anadón, A., Ares, I., 2020. Use of human

neuroblastoma SH-SY5Y cells to evaluate glyphosate-induced effects on oxidative stress, neuronal development and cell death signaling pathways. Environ. Int. 135, 105414. https://doi.org/10.1016/j.envint.2019.105414.
Martini, C.N., Gabrielli, M., Vila, M. del C., 2012. A commercial formulation of glyphosate inhibits proliferation and differentiation to adipocytes and induces apoptosis in 3T3-L1 fibroblasts. Toxicol. Vitr. 26, 1007–1013. https://doi.org/10.1016/j.tiv.2012.04.017.
Martins-Gomes, C., Silva, T.L., Andreani, T., Silva, A.M., 2022. Glyphosate vs. Glyphosate-based herbicides exposure: a review on their toxicity. J. Xenobiotics. https://doi.org/10.3390/jox12010003.
Mesnage, R., Antoniou, M.N., 2022. Molecular toxicity study on glyphosate, Roundup Mon 52276 and a low-dose pesticide mixture administered to adult Female rats for 90 days. Life 15, 1273–1275. https://doi.org/10.1080/26895293.2022.2156626.
Mesnage, R., Benbrook, C., Antoniou, M.N., 2019. Insight into the confusion over surfactant co-formulants in glyphosate-based herbicides. Food Chem. Toxicol. 128, 137–145. https://doi.org/10.1016/j.fct.2019.03.053.
Mesnage, R., Bernay, B., Séralini, G.E., 2013. Ethoxylated adjuvants of glyphosate-based herbicides are active principles of human cell toxicity. Toxicology 313, 122–128. https://doi.org/10.1016/j.tox.2012.09.006.
Mesnage, R., Teixeira, M., Mandrioli, D., Falcioni, L., Ducarmon, Q.R., Zwittink, R.D., Mazzacuva, F., Caldwell, A., Halket, J., Amiel, C., Panoff, J.-M., Belpoggi, F., Antoniou, M.N., 2021. Use of shotgun metagenomics and metabolomics to evaluate the impact of glyphosate or Roundup mon 52276 on the gut microbiota and serum metabolome of sprague-dawley rats. Environ. Health Perspect. 129, 1–15. https://doi.org/10.1289/EHP6990.
Mink, P.J., Mandel, J.S., Sceurman, B.K., Lundin, J.I., 2012. Epidemiologic studies of glyphosate and cancer: a review. Regul. Toxicol. Pharmacol. 63, 440–452. https://doi.org/10.1016/j.yrtph.2012.05.012.
Miyazaki, T., Okada, K., Yamashita, T., Miyazaki, M., 2017. Two-dimensional gas chromatography time-of-flight mass spectrometry-based serum metabolic fingerprints of neonatal calves before and after first colostrum ingestion. J. Dairy Sci. 100, 4354–4364.
Nagy, K., Tessema, R.A., Budnik, L.T., Ádám, B., 2019. Comparative cyto- and genotoxicity assessment of glyphosate and glyphosate-based herbicides in human peripheral white blood cells. Environ. Res. 179, 108851. https://doi.org/10.1016/j.envres.2019.108851.
Pang, Z., Lu, Y., Zhou, G., Hui, F., Xu, L., Viau, C., Spigelman, A.F., MacDonald, P.E., Wishart, D.S., Li, S., Xia, J., 2024. MetaboAnalyst 6.0: towards a unified platform for metabolomics data processing, analysis and interpretation. Nucleic Acids Res. 398–406. https://doi.org/10.1093/nar/gkae253.
Peillex, C., Pelletier, M., 2020. The impact and toxicity of glyphosate and glyphosate-based herbicides on health and immunity. J. Immunotoxicol. 17, 163–174. https://doi.org/10.1080/1547691X.2020.1804492.
Petersen, I.L., Tomasi, G., Sørensen, H., Boll, E.S., Hansen, H.C.B., Christensen, J.H., 2011. The use of environmental metabolomics to determine glyphosate level of exposure in rapeseed (Brassica napus L.) seedlings. Environ. Pollut. 159, 3071–3077. https://doi.org/10.1016/J.ENVPOL.2011.04.005.
Ramirez Haberkon, N.B., Aparicio, V.C., Mendez, M.J., 2021. First evidence of glyphosate and aminomethylphosphonic acid (AMPA) in the respirable dust (PM10) emitted from unpaved rural roads of Argentina. Sci. Total Environ. 773, 145055. https://doi.org/10.1016/j.scitotenv.2021.145055.
Reichenbach, S.E., Tian, X., Boateng, A.A., Mullen, C.A., Cordero, C., Tao, Q., 2013. Reliable peak selection for multisample analysis with comprehensive two-dimensional chromatography. Anal. Chem. 85, 4974–4981. https://doi.org/10.1021/ac303773v.
Ren, J., Yu, Y., Wang, Y., Dong, Y., Shen, X., 2024. Association between urinary glyphosate exposure and cognitive impairment in older adults from NHANES 2013-2014. J. Alzheimer's Dis. 97, 609–620. https://doi.org/10.3233/JAD-230782.
Richard, S., Moslemi, S., Sipahutar, H., Benachour, N., Seralini, G.-E., 2005. Differential effects of glyphosate and Roundup on human placental cells and aromatase. Environ. Health Perspect. 113, 716–720. https://doi.org/10.1289/ehp.7728.
Roberts, E., 1974. γ-aminobutyric acid and nervous system function—a perspective. Biochem. Pharmacol. 23, 2637–2649. https://doi.org/10.1016/0006-2952(74)90033-1.
Rodrigues, S., Menezes, H., Gomes, D., Cardeal, Z., 2024. Impact of exposure to atmospheric particulate matter in human skin-derived fibroblast cells: a metabolomics approach for the class of amino acids based on GC×GC-Q-TOFMS/MS. J. Hazard Mater. 461, 132606. https://doi.org/10.1016/j.jhazmat.2023.132606.
Roma, D., Cecchini, M.E., Tonini, M.P., Capella, V., Aiassa, D., Rodriguez, N., Mañas, F., 2023. Toxicity assessment and DNA repair kinetics in HEK293 cells exposed to environmentally relevant concentrations of Glyphosate (Roundup® Control Max). Toxicol. Res. 12, 970–978. https://doi.org/10.1093/toxres/tfad089.
Rubino, F.M., Pitton, M., Di Fabio, D., Meroni, G., Santaniello, E., Caneva, E., Pappini, M., Colombi, A., 2011. Measurement of S -methylcysteine and S -methyl-mercapturic acid in human urine by alkyl-chloroformate extractive derivatization and isotope-dilution gas chromatography–mass spectrometry. Biomed. Chromatogr. 25, 330–343. https://doi.org/10.1002/bmc.1451.
Sansone, A., Tolika, E., Louka, M., Sunda, V., Deplano, S., Melchiorre, M., Anagnostopoulos, D., Chatgilialoglu, C., Formisano, C., Di Micco, R., Faraone Mennella, M.R., Ferreri, C., 2016. Hexadecenoic fatty acid isomers in human blood lipids and their relevance for the interpretation of lipidomic profiles. PLoS One 11, e0152378. https://doi.org/10.1371/journal.pone.0152378.
Snow, N.H., 2020. Basic Multidimensional Gas Chromatography, first ed. Separation Science and Technology, London.
Song, H.-Y., Kim, Y.-H., Seok, S.-J., Gil, H.-W., Hong, S.-Y., 2012. In vitro cytotoxic effect of glyphosate mixture containing surfactants. J. Korean Med. Sci. 27, 711. https://doi.org/10.3346/jkms.2012.27.7.711.
Sreekumar, A., Poisson, L.M., Rajendiran, T.M., Khan, A.P., Cao, Q., Yu, J., Laxman, B., Mehra, R., Lonigro, R.J., Li, Y., Nyati, M.K., Ahsan, A., Kalyana-Sundaram, S., Han, B., Cao, X., Byun, J., Omenn, G.S., Ghosh, D., Pennathur, S., Alexander, D.C., Berger, A., Shuster, J.R., Wei, J.T., Varambally, S., Beecher, C., Chinnaiyan, A.M., 2009. Metabolomic profiles delineate potential role for sarcosine in prostate cancer progression. Nature 457, 910–914. https://doi.org/10.1038/nature07762.
Szymańska, E., Saccenti, E., Smilde, A.K., Westerhuis, J.A., 2012. Double-check: validation of diagnostic statistics for PLS-DA models in metabolomics studies. Metabolomics 8, 3–16. https://doi.org/10.1007/s11306-011-0330-3.
Tillakaratne, N.J.K., Erlander, M.G., Collard, M.W., Greif, K.F., Tobin, A.J., 1992. Glutamate decarboxylases in nonneural cells of rat testis and oviduct: differential expression of GAD 65 and GAD 67. J. Neurochem. 58, 618–627. https://doi.org/10.1111/j.1471-4159.1992.tb09763.x.
van Den Dool, H., Dec Kratz, P., 1963. A generalization of the retention index system including linear temperature programmed gas-liquid partition chromatography. J. Chromatogr. A 11, 463–471. https://doi.org/10.1016/s0021-9673(01)80947-x.
Villas-Bôas, S.G., Smart, K.F., Sivakumaran, S., Lane, G.A., 2011. Alkylation or silylation for analysis of amino and non-amino organic acids by GC-MS? Metabolites 1, 3–20. https://doi.org/10.3390/metabo1010003.
Wang, B., Habermehl, C., Jiang, L., 2022a. Metabolomic analysis of honey bee (Apis mellifera L.) response to glyphosate exposure. Mol. Omi. 18, 635–642. https://doi.org/10.1039/D2MO00046F.
Wang, X., Lu, Q., Guo, J., Ares, I., Martínez, M., Martínez-Larrañaga, M.-R., Wang, Xu, Anadón, A., Martínez, M.-A., 2022b. Oxidative stress and metabolism: a mechanistic insight for glyphosate toxicology. Annu. Rev. Pharmacol. Toxicol. 62, 617–639. https://doi.org/10.1146/annurev-pharmtox-020821-111552.
Wang, Yuye, Sun, Y., Wang, Yu, Jia, S., Qiao, Y., Zhou, Z., Shao, W., Zhang, X., Guo, J., Song, X., Niu, X., Peng, D., 2023. Urine metabolomics phenotyping and urinary biomarker exploratory in mild cognitive impairment and Alzheimer's disease. Front. Aging Neurosci. 15, 1–10. https://doi.org/10.3389/fnagi.2023.1273807.
Winstone, J.K., Pathak, K.V., Winslow, W., Piras, I.S., White, J., Sharma, R., Huentelman, M.J., Pirrotte, P., Velazquez, R., 2022. Glyphosate infiltrates the brain and increases pro-inflammatory cytokine TNFα: implications for neurodegenerative disorders. J. Neuroinflammation 19, 1–14. https://doi.org/10.1186/S12974-022-02544-5/FIGURES/5.
Wishart, D.S., Guo, A., Oler, E., Wang, F., Anjum, A., Peters, H., Dizon, R., Sayeeda, Z., Tian, S., Lee, B.L., Berjanskii, M., Mah, R., Yamamoto, M., Jovel, J., Torres-Calzada, C., Hiebert-Giesbrecht, M., Lui, V.W., Varshavi, Dorna, Varshavi, Dorsa, Allen, D., Arndt, D., Khetarpal, N., Sivakumaran, A., Harford, K., Sanford, S., Yee, K., Cao, X., Budinski, Z., Liigand, J., Zhang, L., Zheng, J., Mandal, R., Karu, N., Dambrova, M., Schiöth, H.B., Greiner, R., Gautam, V., 2022. Hmdb 5.0: the human metabolome database for 2022. Nucleic Acids Res. 50, D622–D631. https://doi.org/10.1093/nar/gkab1062.
Zhang, Q., Liu, X., Gao, M., Li, X., Wang, Y., Chang, Y., Zhang, X., Huo, Z., Zhang, L., Shan, J., Zhang, F., Zhu, B., Yao, W., 2022. The study of human serum metabolome on the health effects of glyphosate and early warning of potential damage. Chemosphere 298, 134308. https://doi.org/10.1016/j.chemosphere.2022.134308.
Zhang, Z.H., Chen, H., Vaziri, N.D., Mao, J.R., Zhang, L., Bai, X., Zhao, Y.Y., 2016. Metabolomic signatures of chronic kidney disease of diverse etiologies in the rats and humans. J. Proteome Res. 15, 3802–3812. https://doi.org/10.1021/acs.jproteome.6b00583.